Electronically Induced Phase Transitions in Ternary Transition Metal Distannide Systems

Ulrich Häussermann,*,† Sergei I. Simak,‡ Igor A. Abrikosov,‡ Börje Johansson,‡ and Sven Lidin†

Contribution from the Department of Inorganic Chemistry, Stockholm University, 10691 Stockholm, Sweden, and the Department of Condensed Matter Theory, Uppsala University, P.O. Box 530, 75121 Uppsala, Sweden

Received April 20, 1998

Abstract: Our experimental investigation of the quasi-binary systems $Ti_xV_{1-x}Sn_2$, $Ti_xFe_{1-x}Sn_2$, $V_xFe_{1-x}Sn_2$, $Fe_xCo_{1-x}Sn_2$, and $Co_xNi_{1-x}Sn_2$ revealed the interesting sequence of structures $CuMg_2 \rightarrow NiMg_2 \rightarrow CuAl_2 \rightarrow CoGe_2$, where the stability is primarily determined by the valence electron concentration (VEC, number of valence electrons per formula unit). In the range between 12.4 and 14.0 electrons per formula unit, the $CuMg_2$ type has been found to be stable, followed by the $NiMg_2$ type in the region between 13.9 and 14.7 and the $CuAl_2$ type in the region between between 14.7 and 17.1 electrons per formula unit. The three structure types are closely related and represent different stacking sequences of layers consisting of square antiprisms formed by the Sn atoms. The structures of $Ti_{0.62}V_{0.38}Sn_2$ ($CuMg_2$ type) $Ti_{0.4}Fe_{0.6}Sn_2$ ($NiMg_2$ type), $V_{0.75}Fe_{0.25}Sn_2$ ($NiMg_2$ type), and $V_{0.72}Co_{0.28}Sn_2$ ($NiMg_2$ type) were determined by single-crystal X-ray diffraction methods. The structural sequence is completed by the $CoGe_2$ structure type in the system $Co_xNi_{1-x}Sn_2$ when VEC is in the region between 17.2 and 17.6 electrons per formula unit. The theoretical investigation of the systems $Cr_xMn_{1-x}Sn_2$ and $Co_xNi_{1-x}Sn_2$ by the full-potential linear muffin tin orbital method, combined with the virtual-crystal approximation for modeling random occupational disorder of the transition metal atoms, fitted the experimental findings, although the energy differences of the structures $CuMg_2$, $NiMg_2$, and $CuAl_2$ turned out to be very small (less than 0.005 eV/atom in $Cr_xMn_{1-x}Sn_2$). The key role of VEC, that is the band filling, in structural stability for the systems under consideration was confirmed, and the variation of the bonding situation as a function of the band filling was studied by charge density calculations.

Introduction

Electron count plays a pivotal role in the stability of molecular and solid-state structures and is exemplified most impressively by the changes of the elemental structures within the main group periods.[1] On the basis of such observations, chemists have developed powerful rules, such as Wade's rules for deltahedral cluster entities[2] or the (8-N) rule for valence compounds[3] which link electron counts to particular geometrical arrangements. The rules have their theoretical foundations in molecular orbital theory, and a prerequisite for a successful application is that the highest occupied and lowest unoccupied orbitals in molecules are well separated or that solids exhibit a band gap.

Metallic systems evade simple electron-counting schemes and changes in electron count are frequently *not* accompanied by structural changes. In fact, for many systems, large homogeneity ranges exist where one atomic species is replaced by another of similar type or size. Importantly, electron count or synonymously the valence electron concentration (VEC, number of electrons per formula unit) is not the only structure-determining factor in metallic systems, and usually, the difference in electronegativity and the size of the constituting atoms are additionally used to describe structural stability of intermetallic compounds.[4] However, there are systems where structural stability is solely determined by the electron count or VEC and prominent examples are the hcp → bcc → hcp → fcc sequence across the transition metal series[5] or the classic Hume−Rothery (brass) phases in the system $Cu_{1-x}Zn_x$ where the sequence fcc → bcc (β-brass) → γ -brass → hcp is realized with increasing x.[6]

We have focused on a more systematic exploration of the role of electron count or VEC in the stability of intermetallic compounds, especially in the systems T_mE_n with T a transition metal and E a (heavier) p-block element.[7−9] In such systems, changes of VEC can be obtained with only small alterations of the other structure-determining variables (i.e., electronegativity and atomic size difference) when replacing T partly by a second transition metal T′ from the same row. In this article, we report on the interesting structural sequence $CuMg_2 \rightarrow NiMg_2 \rightarrow CuAl_2$

† Stockholm University.
‡ Uppsala University.

(1) Cressoni, J. C.; Pettifor, D. G. *J. Phys.: Condens. Matter* **1991**, *3*, 495.
(2) Wade, K. *Adv. Inorg. Chem. Radiochem.* **1976**, *18*, 1.
(3) (a) Mooser, E.; Pearson, W. B. *Phys. Rev.* **1956**, *101*, 1608. (b) Mooser, E.; Pearson, W. B. *Prog. Semicond.* **1960**, *5*, 103.
(4) Villars, P.; Mathis K.; Hulliger, F. In *The Structure of Binary Compounds*; de Boer F. R., Pettifor, D. G., Eds.; Elsevier: New York, 1989; p 1.
(5) (a) Pettifor, D. G. In *Metallurgical Chemistry*; Kubachewski, O., Ed.; Her Majesty's Stationary Office: London, 1972; p 191. (b) Skriver, H. L. *Phys. Rev. B* **1985**, *31*, 1909.
(6) Hume−Rothery, W.; Raynor, G. V. *The Structure of Metals and Alloys*; Institute of Metals: London, 1962.
(7) Larsson A.-K.; Lidin, S. *J. Alloys Compd.* **1995**, *221*, 136.
(8) Häussermann, U.; Landa-Cánovas, A. R.; Lidin, S. *Inorg. Chem.* **1997**, *36*, 4307.
(9) Häussermann, U.; Elding-Pontén, M.; Svensson, C.; Lidin, S. *Chem. Eur. J.* **1998**, *4*, 1007.

S0002-7863(98)01347-X CCC: $15.00
Published on Web 09/22/1998

Table 1. Crystallographic Data Summary for the Compounds $Ti_{0.62}V_{0.38}Sn_2$, $Ti_{0.4}Fe_{0.6}Sn_2$, $V_{0.75}Fe_{0.25}Sn_2$, and $V_{0.72}Co_{0.28}Sn_2$

	$CuMg_2$ type	$NiMg_2$ type	$NiMg_2$ type	$NiMg_2$ type
chemical formula	$Ti_{0.62}V_{0.38}Sn_2$	$Ti_{0.4}Fe_{0.6}Sn_2$	$V_{0.75}Fe_{0.25}Sn_2$	$V_{0.72}Co_{0.28}Sn_2$
space group	*Fddd* (No. 70)	$P6_222$ (180)	$P6_222$ (180)	$P6_222$ (180)
lattice constants, Å	$a = 5.5682(8)$ $b = 9.643$ (1) $c = 18.918(2)$	$a = 5.4933(5)$ $c = 13.8456(7)$	$a = 5.4556(3)$ $c = 13.8672(8)$	$a = 5.4600(2)$ 13.7965(5)
volume, Å^3	1015.76	361.83	357.44	356.19
Z	16	6	6	6
calc density, g/cm^3	7.492	7.987	8.071	8.127
T, K	295	295	295	295
wavelength, Å^{-1}	0.710 73 (Mo Kα)	0.710 73 (Mo Kα)	0.710 73 (Mo Kα)	0.710 73 (Mo Kα)
absorptions coeff, mm^{-1}	22.38	24.97	24.75	25.14
R1^a [$\|F\|^2 \geq 2\sigma(\|F\|^2)$]	0.023	0.029	0.039	0.022
$R_w{}^b$ [$\|F\|^2 \geq 2\sigma(\|F\|^2)$]	0.043	0.048	0.072	0.041

^{a} $R = [\sum(|F_o| - |F_c|)]/\sum|F_o|$. ^{b} $R_w = \{[\sum w(F_o{}^2 - F_c{}^2)^2]/\sum w(F_o{}^2)^2\}^{1/2}$. $w = [\sigma^2(|F_o|^2 + (aP)^2 + bP]^{-1}$. $P = (F_o{}^2(\geq 0) + 2F_c{}^2)/3$. ($Ti_{0.62}V_{0.38}Sn_2$: $a = 0$, $b = 1.81$. $Ti_{0.4}Fe_{0.6}Sn_2$: $a = 0.011$, $b = 0$. $V_{0.75}Fe_{0.25}Sn_2$: $a = 0.023$, $b = 1.52$. $V_{0.72}Co_{0.28}Sn_2$: $a = 0.007$, $b = 0.80$).

→ $CoGe_2$, which occurs in quasi-binary transition metal distannide systems $T_xT'_{1-x}Sn_2$ (T and T′ from the first transition series) and resembles the structural changes in the Hume–Rothery phases. We combined experimental work and structure elucidation with state-of-the-art computations in the framework of local density functional theory. The full-potential linear muffin tin orbital (FP-LMTO) computations provide the most reliable results for structural predictions when total energies are being compared. Indeed, we were able to model the experimentally observed structural trends and show that band-filling effects are indeed responsible for driving the series of phase transitions in these systems.

Experimental and Calculational Details

Synthesis and Analysis. The quasi-binary systems $Ti_xV_{1-x}Sn_2$, $Ti_x\,Fe_{1-x}Sn_2$, $V_xFe_{1-x}Sn_2$, $V_x\,Co_{1-x}Sn_2$, and $Co_x\,Ni_{1-x}Sn_2$ were studied by preparing samples from a mixture of the pure elements (Ti powder, 99.7%, Aldrich; V powder, 99.5%, Aldrich; Fe powder, 99.9%, Aldrich; Co powder, 99.5%, Kebo; Ni powder, puriss, Fluka; Sn powder, 99.5%, Aldrich) containing a total amount of 1 mmol of transition metal with the following compositions, $x = 0.125, 0.25, 0.375, ..., 0.875$, and an excess of Sn (10 mmol), thus using Sn as reactand and flux medium. The carefully mixed reactands were pressed to pellets and loaded into quarz ampules which were sealed under vacuum. The samples were heated at 650 °C for 3 days and then cooled to room temperature at an approximate rate of 100 °C/h. Excess Sn was dissolved with 4 M HCl. The crystalline remainders, being silvery to dark gray, were characterized by Guinier powder diagrams (Cu Kα) and their compositions analyzed with the energy dispersive X-ray (EDX) method in a JEOL 200 scanning electron microscope. From the analysis of the powder patterns of the samples of the investigated systems, the occurrence of the structure types $CuMg_2$, $NiMg_2$, $CuAl_2$, and $CoGe_2$ was concluded. For systems consisting of a first-row transition metal and tin, the composition TSn_2 represents the Sn-richest compounds, with the exception of $CoSn_3$, which can crystallize in two variants.[10] In our Co-richest samples, we obtained the high-temperature form of $CoSn_3$ with a small amount of Co partly replaced by the second T atom. With increasing T content phases, $T_xCo_{1-x}Sn_2$ with a T/Sn ratio of 1:2 were found as the only products. Crystals of compounds $T_xT'_{1-x}Sn_2$ with different structure types could roughly be distinguished by their different shapes: compounds with the $CuMg_2$ and $NiMg_2$ types preferentially formed hexagon-shaped or rectangular plates, compounds with the $CuAl_2$ type tetragonal rods or needles, and compounds with the $CoGe_2$ type thin rectangular plates. Further, in systems exhibiting phase transitions the different structure types segregated into different regions of existence; i.e., pronounced two-phase regions were detected. Thus, it was possible to distinguish compounds with different structure types by their composition. The limiting compositions of the structure types in the different systems were determined by averaging EDX analyses of 10 different crystals for each phase from the samples exhibiting a two-phase region.

X-ray Structure Determination. Single crystals for X-ray structure determinations were selected from the samples $Ti_{0.625}V_{0.375}$/Sn, $Ti_{0.375}Fe_{0.625}$/Sn, $V_{0.5}Fe_{0.5}$/Sn, $V_{0.5}Co_{0.5}$/Sn, and $Co_{0.625}Ni_{0.375}$/Sn. For all crystals, at least one hemisphere of data was collected at room temperature with Mo Kα radiation (graphite monochromator) on an Enraf Nonius CAD4 diffractometer with the $\omega - 2\theta$ scan type in the range of $2° \leq 2\theta \leq 70°$. Cell constants were obtained from a least-squares refinement of the setting angle of 25 centered reflections. Analytical absorption corrections were applied which improved the quality of all intensity data considerably.[11] The crystal structures were refined using full-matrix least-squares refinement on F^2 (program SHELXL-93.[12] The space group symmetry of $Ti_{0.62}V_{0.38}Sn_2$ ($CuMg_2$ type) is *Fddd* and that of the compounds $Ti_{0.4}Fe_{0.6}Sn_2$, $V_{0.75}Fe_{0.25}Sn_2$, and $V_{0.72}Co_{0.28}Sn_2$ with the $NiMg_2$ type was chosen to be $P6_222$. Refinements in the enantiomorphic space group $P6_422$ yielded the same R values (Table 1) and the same positional and thermal atomic parameters within the standard deviations. Thus, the intensity data are insufficient for distinguishing between $P6_222$ and $P6_422$. Some details of the single-crystal data collection and refinement are listed in Table 1. The composition of the crystals used for X-ray structure determinations was determined from the refined T/T′ ratios. The quality of the intensity data was such that it allowed the refinement of atomic ratios at the mixed transition metal sites, and the refined values agree with the stability ranges of the respective structure types found by EDX analyses of the bulk samples. For the system $Ti_xFe_{1-x}Sn_2$ this may not be surprising, but even in $Ti_xV_{1-x}Sn_2$ the analyzed crystal ($Ti_{0.6}V_{0.4}Sn_2$) is Ti rich at the 0.995 significance level according to Hamilton test. In Table 2, the atomic positions, site occupancies, and isotropic displacement factors are given and in Table 3, the relevant interatomic distances.

FP-LMTO Calculations. The total energies of all structures were calculated by the FP-LMTO method[13] which is a powerful

(10) Lang, A.; Jeitschko, W. *Z. Metallkd.* **1996**, *87*, 759.
(11) *Program TEXSAN*, version 6.0; Molecular Structure Corp.: The Woodlands, TX, 1990.
(12) Sheldrick, G. M. *SHELXL-93 Program for the Refinement of Crystal Structures*; University of Göttingen: Göttingen, Germany, 1993.
(13) (a) Wills, J. M., unpublished information. (b) Wills, J. M.; Cooper, B. R. *Phys. Rev. B* **1987**, *36*, 3809. (c) Price, D. L.; Cooper, B. R. *Phys. Rev. B* **1989**, *39*, 4945.

Table 2. Atomic Coordinates, Occupancies, and Equivalent Isotropic Displacement Parameters (Å^2) for the Compounds $Ti_{0.62}V_{0.38}Sn_2$, $Ti_{0.4}Fe_{0.6}Sn_2$, $V_{0.75}Fe_{0.25}Sn_2$, and $V_{0.72}Co_{0.28}Sn_2$

atom	site	*x*	*y*	*z*	SOF	U_{iso}, 10^4 Å^2
			$Ti_{0.62}V_{0.38}Sn_2$			
T	16 g	1/8	1/8	0.252 55(6)	Ti 0.62(5) V 0.38(5)	68(2)
Sn1	16 g	1/8	1/8	0.538 74(2)	1	116(1)
Sn2	16f	1/8	0.292 37(5)	1/8	1	107(1)
			$Ti_{0.4}Fe_{0.6}Sn_2$			
T1	3b	0	0	1/2	Ti 0.07(4) Fe 0.93(4)	91(5)
T2	3d	1/2	0	1/2	Ti 0.73(4) Fe 0.27(4)	73(5)
Sn1	6f	1/2	0	0.110 44(4)	1	99(1)
Sn2	6i	0.1656(1)	0.3312(2)	0	1	101(1)
			$V_{0.75}Fe_{0.25}Sn_2$			
T1	3b	0	0	1/2	V 0.50(5) Fe 0.50(5)	70(4)
T2	3d	1/2	0	1/2	V 1	50(3)
Sn1	6f	1/2	0	0.110 03(4)	1	79(2)
Sn2	6i	0.1672(1)	0.3344(1)	0	1	78(2)
			$V_{0.72}Co_{0.28}Sn_2$			
T1	3b	0	0	1/2	V 0.44(3) Co 0.56(3)	105(3)
T2	3d	1/2	0	1/2	V 1	76(2)
Sn1	6f	1/2	0	0.110 43(4)	1	99(1)
Sn2	6i	0.166 75(6)	0.3335(1)	0	1	105(1)

Table 3. Selected Bond Distances (Å) in the Compounds $Ti_{0.62}V_{0.38}Sn_2$, $Ti_{0.4}Fe_{0.6}Sn_2$, $V_{0.75}Fe_{0.25}Sn_2$, and $V_{0.72}Co_{0.28}Sn_2$[a]

				$Ti_{0.62}V_{0.38}Sn_2$			
T−T	2.785 × 2			Sn1−T	2.867 × 2	Sn2−T	2.818 × 2
T−Sn2	2.818 × 2			Sn1−T	2.892 × 2	Sn2−T	2.903 × 2
T−Sn1	2.867 × 2			Sn1−Sn1	3.146 × 2	Sn2−Sn2	3.208 × 2
T−Sn1	2.892 × 2			Sn1−Sn1	3.264	Sn2−Sn2	3.228
T−Sn2	2.903 × 2			Sn1−Sn2	3.488 × 2	Sn2−Sn1	3.488 × 2
				Sn1−Sn2	3.599 × 2	Sn2−Sn1	3.599 × 2
				Sn1−Sn2	3.608 × 4	Sn2−Sn1	3.608 × 4
				$Ti_{0.4}Fe_{0.6}Sn_2$			
T1−T2	2.747 × 2	T2−T1	2.747 × 2	Sn1−T1	2.855 × 2	Sn2−T1	2.794 × 2
T1−Sn2	2.794 × 4	T2−Sn2	2.803 × 4	Sn1−T2	2.855 × 2	Sn2−T2	2.803 × 2
T1−Sn1	2.855 × 4	T2−Sn1	2.855 × 4	Sn1−Sn1	3.058	Sn2−Sn2	3.151
				Sn1−Sn1	3.158 × 2	Sn2−Sn2	3.182 × 2
				Sn1−Sn2	3.473 × 2	Sn2−Sn1	3.473 × 2
				Sn1−Sn2	3.516 × 4	Sn2−Sn1	3.516 × 4
				Sn1−Sn2	3.530 × 2	Sn2−Sn1	3.530 × 2
				$V_{0.75}Fe_{0.25}Sn_2$			
T1−T2	2.728 × 2	T2−T1	2.728 × 2	Sn1−T1	2.839 × 2	Sn2−T1	2.795 × 2
T1−Sn2	2.800 × 4	T2−Sn2	2.795 × 4	Sn1−T2	2.839 × 2	Sn2−T2	2.800 × 2
T1−Sn1	2.839 × 4	T2−Sn1	2.839 × 4	Sn1−Sn1	3.052	Sn2−Sn2	3.145 × 2
				Sn1−Sn1	3.148 × 2	Sn2−Sn2	3.160
				Sn1−Sn2	3.473 × 2	Sn2−Sn1	3.473 × 2
				Sn1−Sn2	3.495 × 2	Sn2−Sn1	3.495 × 2
				Sn1−Sn2	3.502 × 4	Sn2−Sn1	3.502 × 4
				$V_{0.72}Co_{0.28}Sn_2$			
T1−T2	2.730 × 2	T2−T1	2.730 × 2	Sn1−T1	2.838 × 2	Sn2−T1	2.787 × 2
T1−Sn2	2.789 × 4	T2−Sn2	2.787 × 4	Sn1−T2	2.838 × 2	Sn2−T2	2.789 × 2
T1−Sn1	2.838 × 4	T2−Sn1	2.838 × 4	Sn1−Sn1	3.047	Sn2−Sn2	3.151 × 2
				Sn1−Sn1	3.140 × 2	Sn2−Sn2	3.155
				Sn1−Sn2	3.456 × 2	Sn2−Sn1	3.455 × 2
				Sn1−Sn2	3.500 × 2	Sn2−Sn1	3.500 × 2
				Sn1−Sn2	3.502 × 4	Sn2−Sn1	3.502 × 4

[a] The standard deviations are all equal or less than 0.001 Å.

all-electron technique in the framework of density functional theory for the calculation of different properties of crystalline materials. Especially, it is considered as one of the most accurate methods concerning structural predictions. The space was divided into so-called muffin tin spheres (MTS) surrounding atomic sites and interstitial regions between them. No approximations were introduced for the shape of the charge density and potential either inside MTS or in the interstitial region. The basis set, charge density, and potential were expanded in spherical harmonic series within nonoverlapping MTS and in Fourier series in the interstitial region. The basis set of augmented linear muffin tin orbitals was used.[14] The tails of

(14) (a) Andersen, O. K. *Phys. Rev. B* **1975**, *12*, 3060. (b) Skriver, H. L. *The LMTO Method*; Springer: Berlin, 1984.

the basis functions outside their parent spheres were linear combinations of Hankel functions with negative kinetic energy. The basis set included 4s, 4p, and 3d orbitals on the sites of 3d metals and 5s, 5p, and 4d orbitals on the Sn sites. All states were contained in the same energy panel. We adopted a double basis where we used two different orbitals of Hankel functions with different kinetic energy. The spherical harmonic expansion of the charge density, potential, and basis functions were carried out to $l = 4$. The integration over the Brillouin zone was performed by the special point sampling[15] with a Gaussian smearing of 20 mRy and using 30, 36, 64, and 68 k-points in the irreducible wedge for the $NiMg_2$, $CuMg_2$, $CuAl_2$, and $CoGe_2$ structures, respectively. The exchange and correlation potential and energy were treated in the local density approximation using the von Barth−Hedin parametrization.[16]

Most conventional methods for the calculation of the electronic structure of crystals, including the here applied FP-LMTO method, have been developed for completely ordered compounds. In the case of partially ordered systems such as $T_xT'_{1-x}Sn_2$, however, one has to deal with atoms of two kinds, T and T′, distributed randomly on some of the sublattices. To handle this problem, we applied the so-called virtual-crystal approximation (VCA), which is the simplest approximation in the hierarchy of mean-field approaches[17] and can be easily combined with a full-potential technique. VCA treats a position on the sublattices occupied by T or T′ as a fictitious atom with the nuclear charge $Z = xZ_T + (1 - x)Z_{T'}$ (where Z_A is the corresponding nuclear charge of the pure element A) and a corresponding number of valence electrons to force charge neutrality. The mean-field treatment is sufficient to describe the case of randomly distributed atoms,[17,18] and in particular, it has been shown that VCA is a suitable approximation for calculating the electronic structure of alloys between neighboring elements in the periodic table.[19] Therefore, we chose the systems $Cr_xMn_{1-x}Sn_2$ and $Co_xNi_{1-x}Sn_2$ for our theoretical investigations. For those systems, we used the structural parameters of the $CuMg_2$, $NiMg_2$, and $CuAl_2$ type observed in the system $Cr_xNi_{1-x}Sn_2$[7] and the structural parameters of the $CuAl_2$ and $CoGe_2$ type observed in the system $Co_xNi_{1-x}Sn_2$[8] as input data. Relaxations with respect to the volume were performed in all the cases, but the positional parameters of the atoms were not further optimized. In the calculations, both systems $Cr_xMn_{1-x}Sn_2$ and $Co_xNi_{1-x}Sn_2$ were treated as being paramagnetic, although in $Cr_xMn_{1-x}Sn_2$ some magnetic ordering occurs in the case of small x values. This, however, does not change the ground-state structure, which was concluded from the results of a number of spin-polarized test calculations.

Experimental Results and Discussion

Structures and Their Homogeneity Ranges. Distannides TSn_2 represent the Sn-richest compounds for the first-row transition metals,[20] with the exception of the system Co/Sn where a dimorphic compound $CoSn_3$ is known.[10] Table 4 gives an overview of the existing compounds and their structures. Three different structure types occur: $ScSn_2$ crystallizes in the recently discovered $ScSn_2$ type,[21] VSn_2 and $CrSn_2$ crystallize in the $CuMg_2$ type, and $MnSn_2$, $FeSn_2$, and $CoSn_2$ crystallize in the $CuAl_2$ type. For Ti and the later transition metals Ni−Zn, the distannide does not exist. During a recent study of the ternary system Cr/Ni/Sn, we obtained a compound $Cr_{0.83}Ni_{0.17}Sn_2$ with the hitherto rarely observed $NiMg_2$ structure and a compound $Cr_{0.75}Ni_{0.25}Sn_2$ with the $CuAl_2$ type.[7] Thus, the small compositional change from $CrSn_2$ to $Cr_{0.75}Ni_{0.25}Sn_2$ gives rise to the structural sequence $CuMg_2 \rightarrow NiMg_2 \rightarrow CuAl_2$, and we suspected the change of VEC from 14 to 15 electrons per formula unit as the driving force. This finding stimulated a more detailed investigation of possible VEC-induced structural changes in systems $T_xT'_{1-x}Sn_2$ with T and T′ being first-row transition metals. The transition metals V−Cu have very similar sizes and electronegativities (cf. Table 4), and their mutual exchange in these quasi-binary systems should basically influence VEC and not the other stability-determining variables, that is, size and electronegativity difference between T and Sn atoms. With this investigation we try to consolidate the idea that VEC (electron count) governs structural stability in the quasi-binary first-row transition metal distannides and commence with the exploration of the homogeneity ranges, that is, ranges of VEC, for the occurring structure types.

Table 4. Selected Properties of the First-Row Transitions Metals

T	atomic vol[a] (Å^3)	EN[b]	structure (TSn_2)	VEC (TSn_2)
Sc	24.97	1.2	$ScSn_2$	11
Ti	17.65	1.3		12
V	13.83	1.5	$CuMg_2$	13
Cr	12.00	1.6	$CuMg_2$	14
Mn	12.21	1.6	$CuAl_2$	15
Fe	11.78	1.6	$CuAl_2$	16
Co	11.07	1.7	$CuAl_2$	17
Ni	10.94	1.8		18
Cu	11.81	1.8		19
Zn	15.21	1.7		20

[a] Values taken from *Binary Alloy Phase Diagrams*, 2nd ed.; ASM International: Materials Park, OH, 1996. [b] EN represents the electronegativity according to Allred and Rochow.

The electron-poorest binary compound with the $CuMg_2$ structure is VSn_2 with a VEC of 13. The system $Ti_xV_{1-x}Sn_2$ offers the possibility to further reduce VEC and thus allows the detection of the lower limit of stability for the $CuMg_2$ type. We could replace V by Ti homogeneously until a limiting composition of $x \approx 0.6$ was reached, corresponding to VEC = 12.4 electrons per formula unit. The structure of a crystal with the composition $Ti_{0.62}V_{0.38}Sn_2$ was refined (Tables 1−3). The system $Ti_xFe_{1-x}Sn_2$ covers a range of VEC between 12 and 16 electrons per formula unit. The $NiMg_2$ structure was found in the range $0.53(1) > x > 0.38(1)$ ($13.9 < \text{VEC} < 14.5$), which corresponds to the limiting compositions $Ti_{53(1)}Fe_{47(1)}Sn_2$ and $Ti_{38(1)}Fe_{62(1)}Sn_2$, and the $CuAl_2$ type was found for $x < 0.12(1)$, i.e., with a limiting composition $Ti_{12(1)}Fe_{88(1)}Sn_2$. The $CuMg_2$ structure was not observed.[22] The systems $V_xFe_{1-x}Sn_2$ and $V_xCo_{1-x}Sn_2$ cover a range of VEC from 13 to 16 and 13 to 17 electrons per formula unit, respectively. We observed the $CuMg_2$ type with the limiting compositions of $V_{0.87(2)}Fe_{0.13(2)}Sn_2$ and $V_{0.89(2)}Co_{0.11(2)}Sn_2$, respectively. The $NiMg_2$ structure

(15) (a) Chadi, D. J.; Cohen, M. L. *Phys. Rev. B* **1973**, *8*, 5747. (b) Froyen, S. *Phys. Rev. B* **1989**, *39*, 3168.
(16) von Barth, U.; Hedin, L. *J. Phys. C* **1972**, *5*, 1629.
(17) See, e.g.: (a) Faulkner, J. S. *Prog. Mater. Sci.* **1982**, *27*, 3. (b) Ducastelle, F. *Order and Phase Stability in Alloys*; North-Holland: Amsterdam, 1991.
(18) Abrikosov, I. A.; Johansson, B. *Phys. Rev. B*, in press.
(19) (a) James, P.; Abrikosov, I. A.; Eriksson, O.; Johansson, B. *Properties of Complex Inorganic Solids*; Gonis, A., Meike, A., Turchi, P. E. A., Eds.; Plenum: New York, 1997; p 57. (b) Abrikosov, I. A.; James, P.; Eriksson, O.; Söderlind, P.; Ruban, A. V.; Skriver, H. L.; Johansson, B. *Phys. Rev. B* **1996**, *54*, 3380.
(20) Villars, P.; Calvert, L. D. *Pearson's Handbook of Crystallographic Data for Intermetallic Compounds*, 2nd ed.; ASM International: Materials Park, OH, 1991.
(21) Pani, M.; Manfrinetti, P.; Fornasini, M. L. *Acta Crystallogr., Sec. C* **1995**, *C51*, 1725.
(22) Samples with higher Ti content than $x = 0.6$ yielded mixtures of $Ti_xFe_{1-x}Sn_2$ with the $NiMg_2$ type and Ti_6Sn_5.

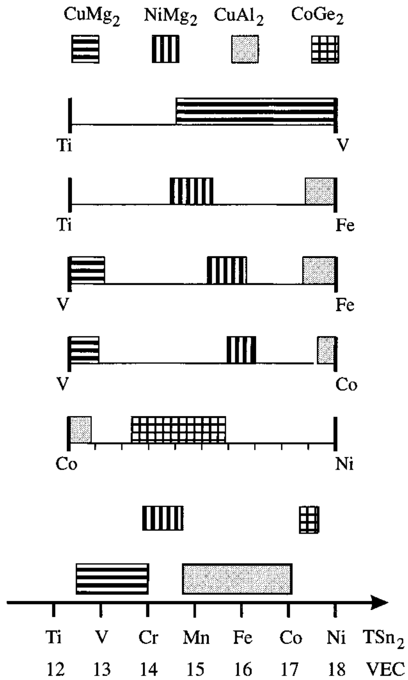

Figure 1. Experimentally determined homogeneity ranges of the structure types $CuMg_2$, $NiMg_2$, $CuAl_2$, and $CoGe_2$ in the pseudo-binary systems $Ti_xV_{1-x}Sn_2$, $Ti_xFe_{1-x}Sn_2$, $V_xFe_{1-x}Sn_2$, $Fe_xCo_{1-x}Sn_2$, and $Co_xNi_{1-x}Sn_2$.

was found in the range $0.67(3) > x > 0.52(2)$ ($14 < VEC < 14.5$) in the system $V_xFe_{1-x}Sn_2$ and in the range $0.70(3) > x > 0.59(3)$ ($14.2 < VEC < 14.6$) in the system $V_xCo_{1-x}Sn_2$, and finally, the $CuAl_2$ type was found with the limiting compositions of $V_{0.13(2)}Fe_{0.87(2)}Sn_2$ and $V_{0.07(2)}Co_{0.93(2)}Sn_2$, respectively. Remarkably, it was possible to obtain the rare $NiMg_2$ structure[23] in several different systems by adjusting an appropriate VEC which is between 14 and 14.7 electrons per formula unit. The refined single-crystal X-ray structures of $Ti_{0.4}Fe_{0.6}Sn_2$ (VEC = 14.4), $V_{0.75}Fe_{0.25}Sn_2$ (VEC = 13.8, note that this value is slightly below the lower limit found by the EDX analyses), and $V_{0.72}Co_{0.28}Sn_2$ (VEC = 14.1) are presented in Tables 1−3. We could not obtain the $NiMg_2$ structure in the system $Cr_xMn_{1-x}Sn_2$. Samples with the proper composition $Cr_{0.5}Mn_{0.5}$/Sn yielded a mixture of $Cr_xMn_{1-x}Sn_2$ with the $CuAl_2$ type ($x \approx 0.3$) and elemental Cr. However, we observed that reactions in samples containing Cr were frequently not complete. The electron-richest binary compound is $CoSn_2$ with the $CuAl_2$ structure (cf. Table 1). The system $Co_xNi_{1-x}Sn_2$ was used to increase VEC above the value of 17 in order to detect the upper limit of stability for the $CuAl_2$ type. We found a limiting composition of $Co_{0.93(2)}Ni_{0.07(2)}Sn_2$ for the $CuAl_2$ type corresponding to VEC = 17.1. At still higher values of VEC ($17.2 < VEC < 17.6$) in the system $Co_xNi_{1-x}Sn_2$ ($0.41 < x < 0.77$), the structure types $CoGe_2$ and $PdSn_2$ occur. We reported earlier on the dimorphism of this phase.[8]

Figure 1 summarizes the experimentally obtained homogeneity ranges of the different structure types, which establishes the clear structural trend $CuMg_2 \rightarrow NiMg_2 \rightarrow CuAl_2 \rightarrow CoGe_2$ with increasing VEC. The $CuMg_2$ type was found to be stable in the range between 12.4 and 14 electrons per formula unit, followed by the $NiMg_2$ type in the region between 13.9 and 14.7 electrons per formula unit and the $CuAl_2$ type in the region between between 14.7 and 17.1 electrons per formula unit.

(23) Besides $NiMg_2$ only $MoSn_2$[26] and the investigated pseudobinary distannides are known to adopt this structure.

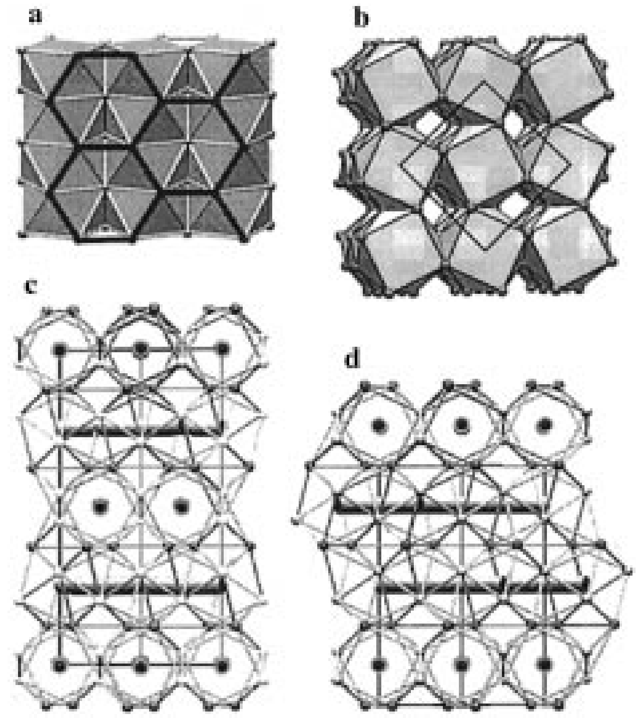

Figure 2. (a) Common building block of the structure types $CuAl_2$, $CuMg_2$, and $NiMg_2$. Stacking variants based on this building block: $CuAl_2$, AA′ stacking (b); $CuMg_2$, AA′BB′ stacking (c); $NiMg_2$, ABC stacking (d). The linear chains of T atoms in $CuMg_2$ and $NiMg_2$ are emphasized as a guide for the eye. The two kinds of E atoms occurring in these structures are distinguished by light (E1 atoms) and dark gray (E2 atoms) of the spheres.

Finally, the $CoGe_2$ ($PdSn_2$) structure appears when VEC reaches values between 17.2 and 17.6 electrons per formula unit.

Structural Relationships. The structure types $CuAl_2$, $CuMg_2$, and $NiMg_2$ are closely related, which was first recognized by Schubert[24] and described in detail by Gingl et al.[25] and Wölpl and Jeitschko.[26] The common building block of the structures is a slab consisting of strands of square antiprisms which are formed by the Sn atoms (Figure 2a). Within a single strand, square antiprisms are connected via common square faces, and in the slab, the strands are oriented parallel and joined together by sharing common prism edges. The antiprisms are centered by the T atoms, which are thus arranged in parallel oriented linear chains within the building block. As a distinctive characteristic, the building block is bounded by honeycomb nets on the surface (outlined in Figure 2a), and on the basis of this building block, the structures $CuAl_2$, $CuMg_2$, and $NiMg_2$ can now easily be described as stacking variants. The honeycomb net as junction unit allows three different orientations of the blocks when they are rotated mutually by 120, 240, or 360°. The $CuAl_2$ structure (tI12[27]) is formed when building blocks are stacked in the same orientation. The stacking direction corresponds to the [110] direction in the tetragonal structure

(24) Schubert, K. *Kristallstrukturen zweikomponentiger Systeme*; Springer: Berlin, 1964; p 288.

(25) Gingl, F.; Selvam, P.; Yvon, K. *Acta Crystallogr., Sec. B* **1993**, *B49*, 201.

(26) (a) Wölpl, T.; Jeitschko, W. *J. Alloys Compd.* **1994**, *210*, 185. (b) Wölpl, T.; Jeitschko, W. *Z. Anorg. Allg. Chem.* **1994**, *620*, 467.

(27) The Pearson symbolism for the classification of crystal structures uses the three quantities *l*, *M*, *n*: *l* denotes the crystal system (c = cubic, h = hexagonal (rhombohedral), t = tetragonal, o = orthorhombic, m = monoclinic, a = anorthic (triclinic)), *M* represents the Bravais type (*P* = primitive, I = body-centered, F = face-centered, R = rhombohedral, A, B, C = single face-centered), and *n* is the number of atoms in the unit cell.

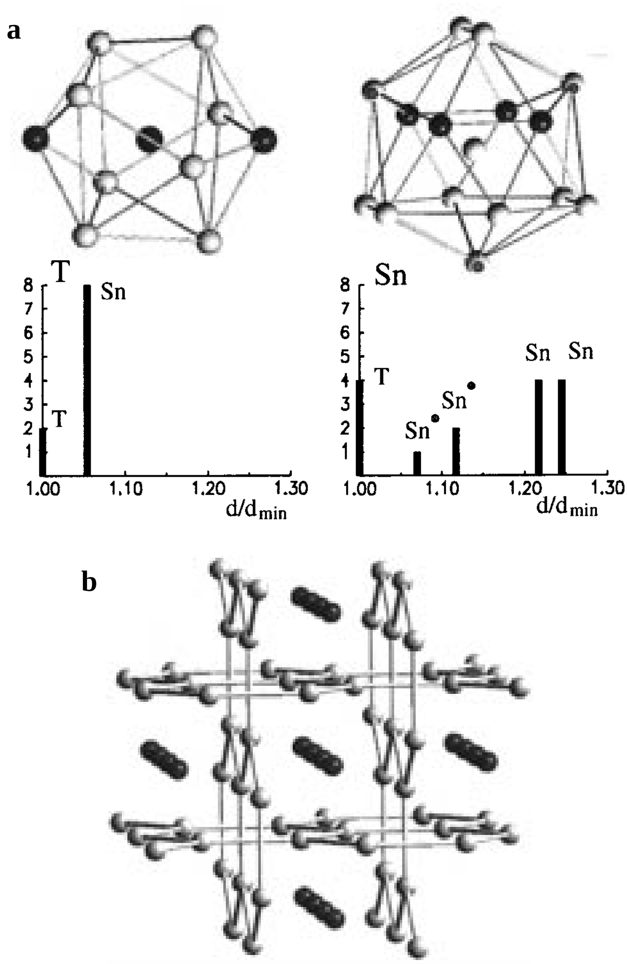

Figure 3. Coordination polyhedra together with nearest-neighbor histograms (a) and the Sn atom partial structure (b) typical of transition metal distannides with the $CuAl_2$ structure. In the histograms, the distances are normalized with respect to the shortest nearest-neighbor distance. T atoms are represented as black; Sn atoms as light gray circles.

and the honeycomb nets are situated on mirror planes (Figure 2b). Thus, the stacking sequence is AA′ where the prime distinguishes reflected building blocks. In the orthorhombic $CuMg_2$ structure (oF48), the stacking sequence is ABA′B′ along the *c* direction (Figure 2c). In this structure, consecutive building blocks with the same orientation are shifted with respect to each other and are distinguished by the prime. Finally, in the hexagonal $NiMg_2$ structure (hP18), building blocks are stacked with the sequence ABC in the *c* direction (Figure 2d).

In the $CuAl_2$ type, only one kind of T and one kind of E atom are present and the coordination polyhedra are shown in Figure 3a. Additionally, the nearest-neighbor histograms typical for first-row transition metal distannides with this structure (E = Sn) are shown (structural parameters taken from ref 7). The T atoms have 10 neighbors at almost equal distances whereas the coordination sphere of the E atoms consists of 7 nearest neighbors (4 T atoms and 3 E atoms) and 8 additional E atoms at a slightly larger distance. In the distannides with the $CuAl_2$ type, the shortest distances between Sn atoms represent the honeycomb net and the Sn partial structure based on these contacts consists of two sets of perpendicularly oriented, interpenetrating honeycomb nets as shown in Figure 3b. In the $CuMg_2$ structure, two different kinds of E atoms occur. One sort of atom (the E2 atoms; cf. Table 2 and Figure 2c) forms the honeycomb nets and the E1 atoms complete these nets to slabs of square antiprisms. The coordination polyhedron of E1 corresponds to one of the E atoms in the $CuAl_2$ structure, whereas that of the E2 atoms is slightly different as concerns the arrangement of the T atoms (Figure 4a). The nearest-neighbor histograms of E1 and E2 are almost identical. The E partial structure based on the closest set of E–E contacts is remarkable (Figure 4b). There are no short E1–E2 distances. Thus, the E2 atoms form isolated honeycomb nets stacked in the *c* direction. These nets are interpenetrated by a framework of E1 atoms in which these atoms—like the E2 atoms of the honeycomb net—are three-coordinated in a trigonal planar way. The resulting arrangement corresponds to the Si partial structure in the $ThSi_2$ type. Finally, in the $NiMg_2$ structure, T and E atoms each occupy two crystallographically different positions. The coordination polyhedra of the two kinds of E atoms correspond to those of the E atoms in the $CuMg_2$ structure. Again, when considering the E partial structure based on closest E–E contacts, one sort of E atom (the E2 atoms) forms the honeycomb nets and the other sort of E atom forms an interpenetrating three-connected net. In this net, however, the zigzag chains of E atoms are mutually rotated by 120° along the direction of the *c* axis (Figure 4c), whereas in $CuMg_2$ ($ThSi_2$), consecutive chains are mutually rotated by 90°. Interestingly, the three-connected net of the E1 atoms in the $NiMg_2$ type is also the basis of the B_2O_3 structure.[28] Thus, the E atoms of the three structure types $CuAl_2$, $CuMg_2$, and $NiMg_2$ form the three basic three-connected nets. Proceeding with the two kinds of T atoms in $NiMg_2$, their nearest-neighbor coordinations are obviously identical (cf. Tables 2 and 3), but in the investigated ternary systems, we found a pronounced tendency of the transition metal atoms to segregate on the two positions. Considering the compounds with the pairs of T atoms Ti/Fe, V/Fe, V/Co (Table 2) and Cr/Ni[7] the more electron-rich T atom in a pair (cf. Table 4) preferentially occupies the T1 positions. These four ternary compounds with the $NiMg_2$ structure have all very similar positional parameters and *c*/*a* ratios, and thus, we consider that this remarkable ordering effect is due to slight differences in the next nearest-neighbor environments (Figure 5).

The orthorhombic $CoGe_2$ structure is clearly distinct from the group $CuAl_2$, $CuMg_2$, and $NiMg_2$ but can be easily derived from the $CuAl_2$ type. Figure 6a shows the $CuAl_2$ structure projected along the c direction. The strands of square antiprisms appear now to be constituted of 3^2 434 nets which are stacked on top of each other, alternately arranged in antiposition. When substituting every second 3^2 434 net by a 4^4 (square) net (Figure 6b), the building block A of the $CoGe_2$ type is obtained (Figure 6c). In the complete structure, the building blocks are mutually shifted by (1/2,0,0) and stacked in an AB sequence in the c direction (Figure 6d). Thus, the infinite chains of T atoms in the $CuAl_2$ structure is broken into pairs in the $CoGe_2$ structure and their E coordination polyhedron is between a cube and a square antiprism. The E atoms forming the 4^4 net are coordinated approximately like the F atoms in the fluorite structure (CaF_2; i.e., these atoms are surrounded tetrahedrally by T (Ca) atoms and (approximately) octahedrally by E (F) atoms) at a slightly larger distance) and the nearest-neighbor arrangement of the other set of E atoms (the $3^2$434 net) consisting of four T atoms and three E atoms is only slightly different from that of the E atoms in $CuAl_2$ (cf. Figure 6a and b). Thus, the $CoGe_2$ structure might be considered as a hybrid between the fluorite and the $CuAl_2$ structure.[29]

(28) Wells, A. F. *Structural Inorganic Chemistry*, 4th ed.; Clarendon Press: Oxford, 1975; p 96.
(29) Hellner, E. *Z. Kristallogr.* **1956**, *107*, 99.

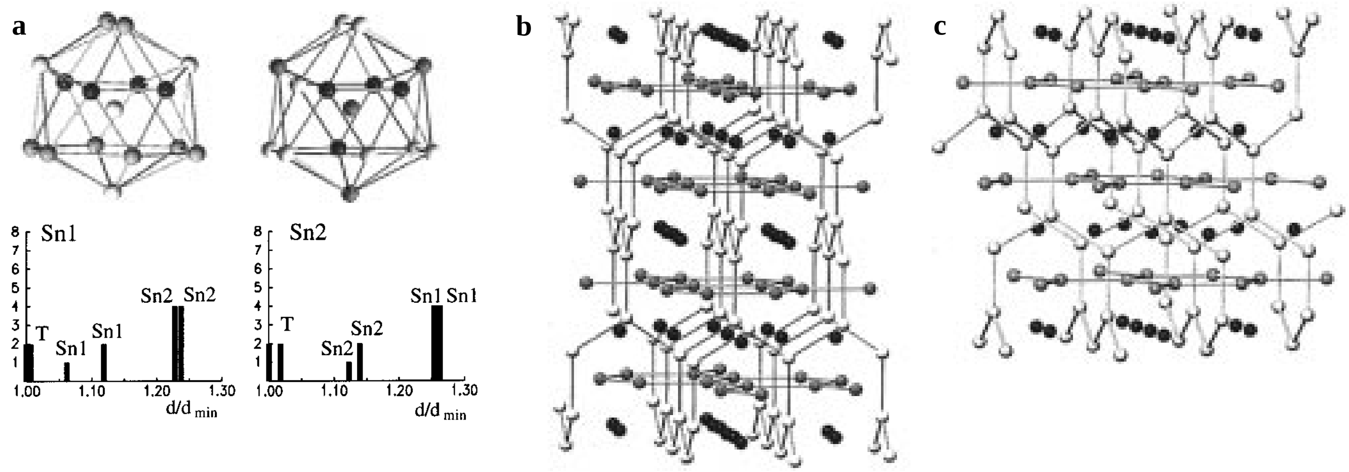

Figure 4. (a) Coordination polyhedra of the Sn atoms together with nearest-neighbor histograms of $CrSn_2$ with the $CuMg_2$ structure. (b) The Sn atom partial structure in $CrSn_2$ with the $CuMg_2$ structure. (c) The Sn atom partial structure in $Cr_{0.83}Ni_{0.17}Sn_2$ with the $NiMg_2$ structure. T atoms are displayed in black, Sn1 atoms in light gray, and Sn2 atoms in dark gray.

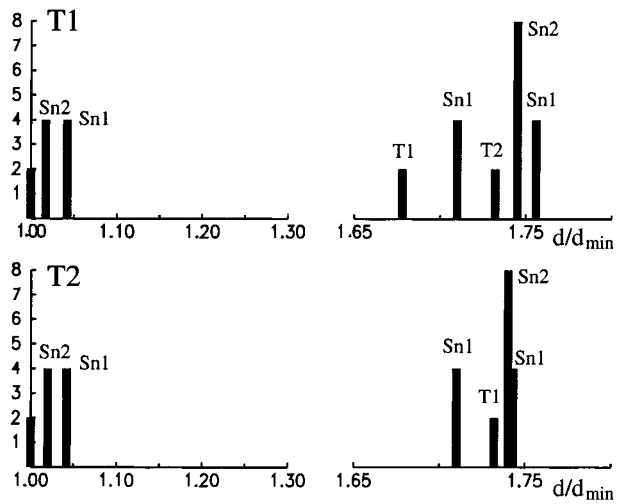

Figure 5. Nearest-neighbor histograms for the two kinds of T atoms in the $NiMg_2$ structure of $Cr_{0.83}$ $Ni_{0.17}$ Sn_2.[7]

In the subsequent theoretical investigation, we try to understand the reason behind the apparent electronically induced phase transitions or, alternately, the role of VEC (electron count) in the stability sequence of the structure types $CuMg_2 \rightarrow NiMg_2 \rightarrow CuAl_2 \rightarrow CoGe_2$ in the transition metal distannide systems.

Theoretical Results and Discussion

Structural Energy Differences and Stability. To model the first group of phase transitions occurring in the region of VEC between 14 and 15 electrons per formula unit, we investigated the system $Cr_xMn_{1-x}Sn_2$ and performed FP-LMTO total energy calculations for the compounds $CrSn_2$, $Cr_{0.75}Mn_{0.25}Sn_2$, and $MnSn_2$ in the three structure types $CuMg_2$, $NiMg_2$, and $CuAl_2$. For modeling the transition $CuAl_2 \rightarrow CoGe_2$ energy vs volume curves for the compounds $CoSn_2$ and $Co_{0.5}Ni_{0.5}Sn_2$ in the $CuAl_2$ and $CoGe_2$ structures were calculated. In the ternary compounds $Cr_{0.75}Mn_{0.25}Sn_2$ and $Co_{0.5}Ni_{0.5}Sn_2$, the T atoms were assumed to be randomly distributed on their atomic sites, which was approached by applying the VCA (cf. Calculational Details). Figure 7 summarizes the obtained total energy curves as a function of volume together with the experimental findings.

For the compound $CrSn_2$, the $CuMg_2$ type is found to be the most stable structure in accord with experiment. The $NiMg_2$ and the $CuAl_2$ type are ~0.005 and 0.01 eV/atom less stable, respectively. It has to be pointed out that these differences in total energy are very small, corresponding to ~50 K.[30,31] Even smaller is the range of total energies for the three structure types at their equilibrium volumes for the compound $Cr_{0.75}Mn_{0.25}Sn_2$. The total energies differ by no more that 0.004 eV/atom. Now the $NiMg_2$ structure is most stable, as would be predicted from the experimental results for a VEC of 14.25. However, the stabilization against the $CuMg_2$ type is only 0.001 eV/atom, which is at the accuracy limits of the FP-LMTO method. The possible segregation of the two different T atoms in this structure type leads to an intriguing stabilization of the $NiMg_2$ structure (shown in the inset of the part of Figure 7 dealing with the phase $Cr_{0.75}Mn_{0.25}Sn_2$). The total energy of $Cr_{0.75}Mn_{0.25}Sn_2$ with the T2 position exclusively being occupied by Cr atoms and the T1 position half-occupied by Cr and Mn atoms is ~0.009 eV/atom lower than the energy of $Cr_{0.75}Mn_{0.25}Sn_2$ with both T atom positions randomly occupied by Cr and Mn atoms. On the other hand, an inverse segregation of the T atoms leads to a destabilization by 0.009 eV/atom. The possibility of segregating T atoms differently yields an energetic effect ($\Delta E \approx 0.018$ eV/atom) more than 4 times as high as is obtained from structural variations based on different stacking sequences ($\Delta E \approx 0.004$ eV/atom) for the particular system $Cr_{0.75}Mn_{0.25}Sn_2$. (Note that the atomic positions were not optimized.) This coincides exactly with the experimentally found tendency of the more electron-rich transition metal in the pair T/T′ to preferentially occupy the T1 position. For the compound $MnSn_2$, the $CuAl_2$ type is calculated to be most stable and this is also the experimentally found structure. The $NiMg_2$ and the $CuMg_2$ types are higher in energy by ~0.005 and 0.01 eV/atom, respectively; i.e., the energy separation of the structures corresponds approximately to that found for $CrSn_2$. Proceeding with the transition $CuAl_2 \rightarrow CoGe_2$ at high values of VEC, it is realized that for the compound $CoSn_2$ the $CuAl_2$ structure is clearly favored against the $CoGe_2$ type (by ~0.03 eV/atom). At a VEC of 17.5, corresponding to the compound $Co_{0.5}Ni_{0.5}Sn_2$, the $CoGe_2$ structure has become more stable than the $CuAl_2$ structure (by more that 0.01 eV/atom). Here the local coordination of some atoms is changed during the transition and we

(30) Note that, for comparison, the fcc−hcp energy differences of the transition metals are in the range of 0.03 eV/atom. For Cu, this difference is smallest and the fcc structure is only stable by less than 0.007 eV/atom.[31]

(31) Paxton, A. T.; Methfessel, M.; Polatoglou, H. M. *Phys. Rev. B* **1990**, *41*, 8127.

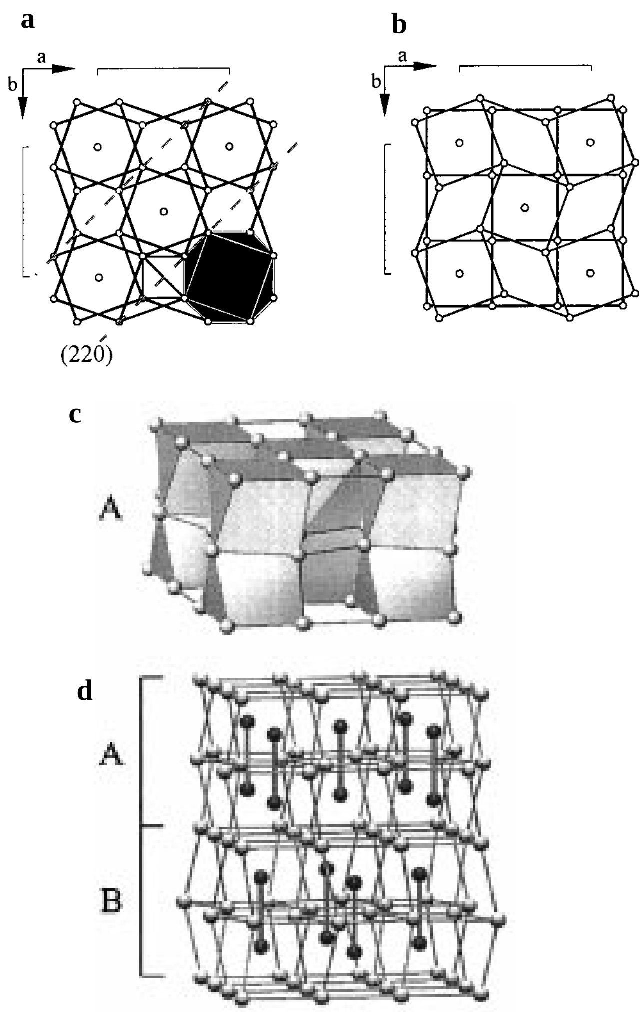

Figure 6. (a) The $CuAl_2$ structure as composed from 3^2434 nets stacked along the c direction. The planes (220) containing the E atom honeycomb nets are indicated. (b) Arrangement of alternately stacked 3^2434 and 4^4 nets. Circles in the net corners denote E atoms; circles in the center of the squares represent T atoms. (c) Building block of the $CoGe_2$ structure. (d) The structure of $CoGe_2$ with AB stacked building units along the c direction. The pairs of T atoms are represented as joined dark circles.

obtain considerably larger differences in total energy between these two structures for compositions distinct from the transition point. As a conclusion the FP-LMTO total energy calculations, which refer to the situation at absolute zero, confirm nicely to the experimentally observed structural trends (Figure 7).

Band Filling and Structural Changes. The investigated distannide systems can accommodate a variable electron count over an extended interval until a structural change is observed. This phenomenon is frequently observed in metallic systems and is in contrast to semiconducting or insulating systems where a change of VEC typically leads directly to a structural transformation. Furthermore, in metallic systems, VEC-induced transitions only may result in small structural changes leaving the nearest-neighbor environment of the atoms practically unchanged, which is realized, for example, in different stacking variants of a common building block. In semiconducting or insulating systems, changes in electron count are often accompanied by a formation or breakage of bonds; i.e., the structural change involves the first coordination sphere. When a structural transition just alters the stacking sequence in two structures, as was found for the transformations $CuMg_2 \rightarrow NiMg_2 \rightarrow CuAl_2$, the associated changes in the total energy are very small, which makes it difficult to explain such a transformation from a chemical point of view. In simple cases, such as the fcc−hcp structural competition of the transition metals, the moments theorem by Ducastelle and Cyrot-Lackmann[32] can provide a chemically transparent explanation but it is hardly applicable to the much more complex structures $CuMg_2$, $NiMg_2$, and $CuAl_2$. The same problem is encountered with the prominent Hume−Rothery phases, although it was recently shown that the Hume−Rothery electron concentration rules can be nicely modeled with simple tight-binding theory.[33] Therefore, the interpretation of the structural trend of these phases is usually treated in a physical way, and the stability sequence is attributed to so-called van Hove singularities in the density of states.[34] These singularities arise when the band structure has zero slope and are recognized as spikey peaks in the density of states. If the Fermi level of a compound coincides with such a singularity, an instability is *indicated* because a splitting of electronic states around the Fermi energy (i.e., a partly lowering and rising of levels) always decreases the one-electron term of the total energy and thus often stimulates changes in the system. A reduced density of states at the Fermi level can be obtained, for example, by a distortion, a structural change, phase separation, or the occurrence of magnetism. For the Hume−Rothery phases, van Hove singularities in the density of states of the different structures appear successively as VEC is increased. In principle we can apply the same kind of argumentation to explain the sequence $CuMg_2 \rightarrow NiMg_2 \rightarrow CuAl_2$ of structural transformations in the transition metal distannide systems when examining the density of states curves obtained from the FP-LMTO calculations (Figure 8).

First it is realized that the density of states of the three structure types $CuAl_2$, $CuMg_2$, and $NiMg_2$ for the different compounds reflect their great similarity, namely, that they represent stacking variants of a common building block with virtually the same nearest-neighbor coordination of the atoms. The structure of $CuAl_2$ corresponds to the simplest stacking possibility and, taking its density of states as a reference, those of the more complicated stacked structures $CuMg_2$ and $NiMg_2$ appear just as “fine-structured” derivatives of the $CuAl_2$ density of states. This fine structure produces pronounced local minimums in the regions below 15 electrons per formula unit when the density of states of the three structure types are compared, and this is the reason behind the delicate differences in the structural energies. Starting with low values of VEC, the $CuMg_2$ structure is the ground state, as for example for the compound $CrSn_2$ with VEC = 14 (upper left corner in Figure 8). Just above the Fermi level of $CrSn_2$, a pronounced van Hove singularity is recognized, and in the compound $Cr_{0.75}Mn_{0.25}Sn_2$ with VEC = 14.25, the Fermi level cuts exactly this singularity in the density of states of the $CuMg_2$ type. As a consequence, the system transforms from the $CuMg_2$ structure into the $NiMg_2$ type. For $Cr_{0.75}Mn_{0.25}Sn_2$ in the $NiMg_2$ structure, the Fermi level is situated precisely between two singularities. The effect of the possible segregation of the T atoms on two different positions can be studied in Figure 9. When the T atoms are distributed according to the experimentally observed and stabilizing trend, the density of states just below the Fermi level in the region between −0.1 and −0.6 eV is only slightly rearranged, which nevertheless accounts for a rather large energetic effect. We consider the possibility of segregation of

(32) (a) Ducastelle, F.; Cyrot-Lackmann, F. *J. Phys. Chem. Solids* **1971**, *32*, 285. (b) Burdett, J. K.; Lee, S. *J. Am. Chem. Soc.* **1985**, *107*, 3050.
(33) Hoistad, L. M.; Lee, S. *J. Am. Chem. Soc.* **1991**, *113*, 8216.
(34) Pettifor, D. G. *Bonding and Structure of Molecules and Solids*; Oxford University Press: New York, 1995; p 166.

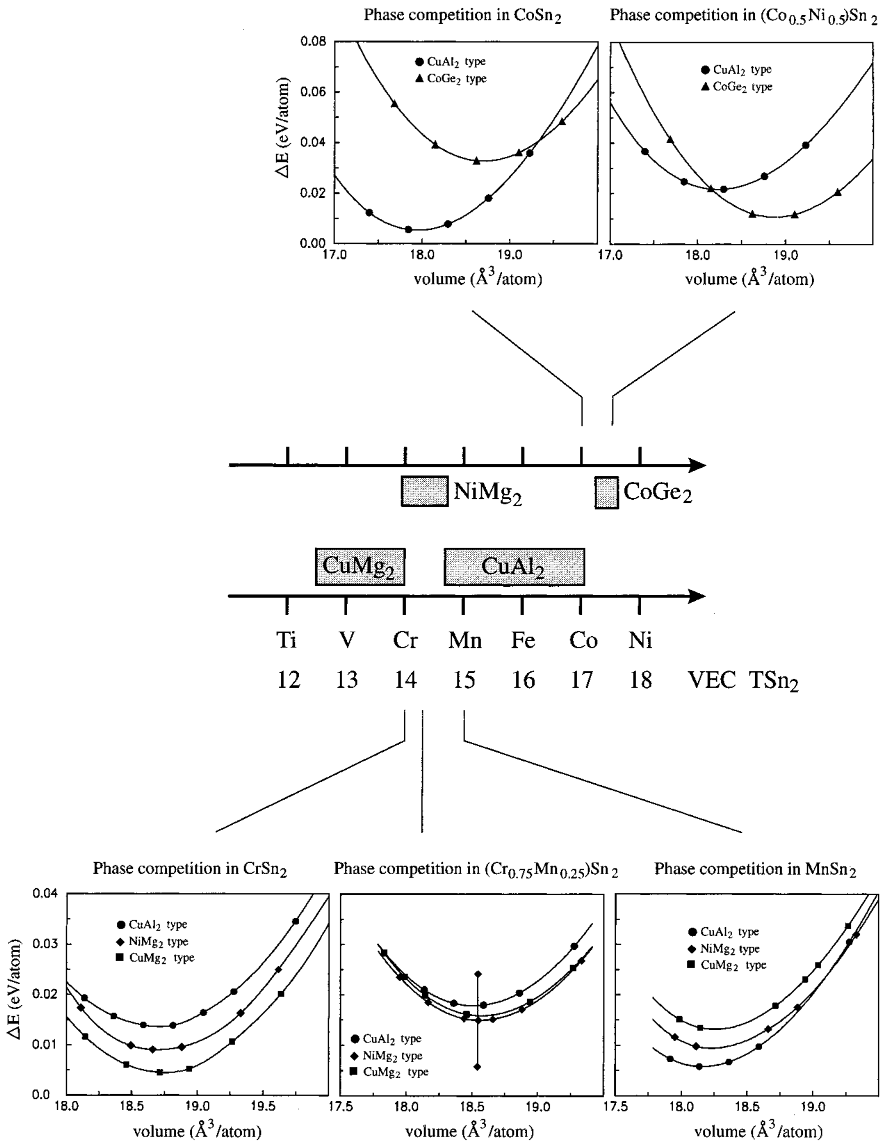

Figure 7. Collection of the experimental results and the theoretical results obtained from FP-LMTO calculations (total energy vs volume curves). The diagram concerning the phase $Cr_{0.75}Mn_{0.25}Sn_2$ also contains the total energies of the $NiMg_2$ structure with T atoms segregated on the two different positions. Lowest in energy is the distribution T1 = 50% Cr/50% Mn, T2 = 100% Cr; highest in energy the distribution T1 = 100% Cr, T2 = 50% Cr/50% Mn.

the T atoms in the $NiMg_2$ structure as a decisive stabilization effect against the other two structure types $CuAl_2$ and $CuMg_2$. Quasi-binary systems offer, besides the adjustment of an appropriate VEC, this possibility. With a further increase of VEC, the van Hove singularity marked with an arrow in Figure 9 is crossed. This singularity may designate the stability boundary for the $NiMg_2$ structure in the system $Cr_xMn_{1-x}Sn_2$, and at higher electron counts, the $CuAl_2$ type emerges as the most stable structure. The $CuAl_2$ structure exhibits the largest stability interval with respect to electron count. Above the Fermi level of $MnSn_2$, a set of more broad maximums in the density of states is located (Figure 8). The occupation of the corresponding bands, which have predominantly 3d character, is not accompanied by any structural change for $FeSn_2$ and $CoSn_2$. For $FeSn_2$, however, they represent a pronounced van Hove singularity and indeed this compound is reported to be antiferromagnetic.[35] In $CoSn_2$ with the $CuAl_2$ structure, the flat bands are completely occupied (Figure 8, lower part). When the VEC is even further increased, as is realized in the system $Co_xNi_{1-x}Sn_2$, the van Hove singularity in the density of states located at ~0.5 eV is reached and the $CoGe_2$ structure emerges. This structure is found to be stable until a limiting composition $Co_{0.59}Ni_{0.41}Sn_2$. The singularity just above the Fermi level of $Co_{0.5}Ni_{0.5}Sn_2$ with the $CoGe_2$ structure (Figure 8, lower part) coincides with the electron count of this limiting composition and could explain the experimentally observed phase separation into $Co_{0.59}Ni_{0.41}Sn_2$ and $Ni_{3-x}Co_xSn_4$ above this point.[8]

It is important to note that the band structure of the different structure types cannot be described by a complete rigid-band behavior but changes slightly when the electron count (i.e., the ratio of the transition metals) of a particular system is varied and even more when quasi-binary systems of different elemental composition are compared with each other. This is evident from the differences in the density of states of the compounds $MnSn_2$ and $CoSn_2$ in the $CuAl_2$ structure (Figure 8). The location of the van Hove singularities determines the stability ranges of the particular structure types and might even account for the ranges of the two-phase regions where a phase separation is

(35) Djega-Mariadassou, C.; Lecocq, P.; Michel, A. *Ann. Chim.* **1969**, *3*, 175.

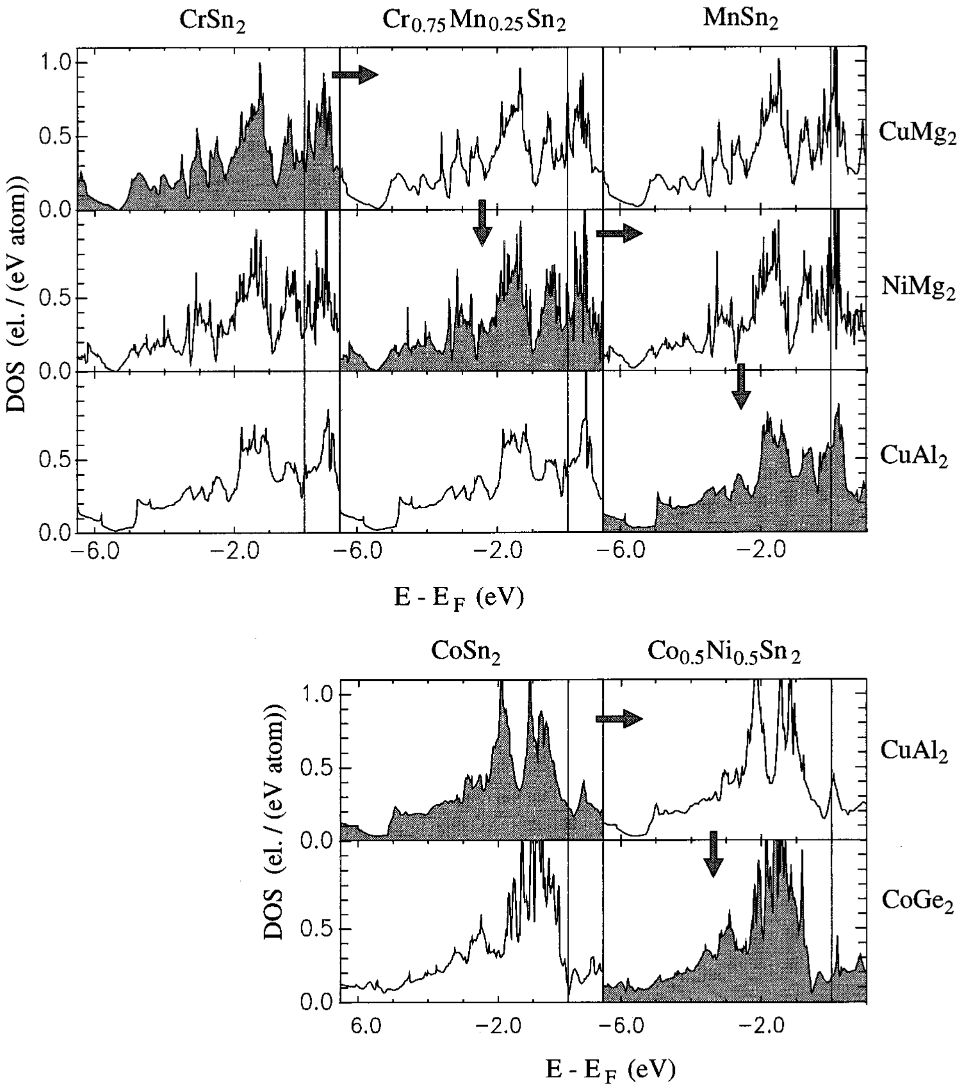

Figure 8. Total density of states (DOS) for the systems $Cr_xMn_{1-x}Sn_2$ and $Co_xNi_{1-x}Sn_2$ obtained from FP-LMTO calculations. The curves of the ground-state structures are emphasized, and the path of structural transformations is marked with arrows.

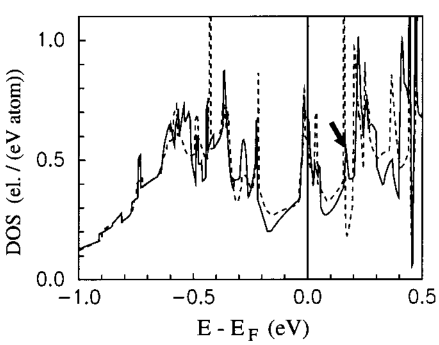

Figure 9. Total Density of States (DOS) for the system $Cr_{0.75}Mn_{0.25}$-Sn_2 with T1 = T2 = 75% Cr/25% Mn (broken line) and T1 = 50% Cr/50% Mn, T2 = 100% Cr (solid line).

observed. In the investigated systems $Ti_xFe_{1-x}Sn_2$, $V_xFe_{1-x}Sn_2$, and $V_xCo_{1-x}Sn_2$, these ranges were found to be slightly different (cf. Figure 1).

Band Filling and Chemical Bonding. How is the local chemical bonding affected by the band filling? To answer this question we analyzed the charge density ρ in $MnSn_2$, $CoSn_2$, and $Co_{0.5}Ni_{0.5}Sn_2$ with the $CuAl_2$ structure. The charge density was calculated in the plane (220) containing the honeycomb net of Sn atoms, in the plane (001) which hosts the 3^2434 net of Sn atoms and bisects the distance between the chain-forming T atoms (cf. Figure 6a), and in a plane defined by a triangle consisting of two T atoms within a chain and a Sn atom situated closest to such two T atoms. The result for $MnSn_2$ is shown in Figure 10a. The (220) plane (Figure 10a top, left) reveals directional bonding between pairs of Sn atoms defining the honeycomb net. Thus the Sn partial structure consisting of two sets of perpendicularly oriented, interpenetrating honeycomb nets (Figure 3b) represents a bonded arrangement with a Sn atom coordinated in a trigonal planar way by three other tin atoms. (Note that the conventional coordination polyhedron is larger, containing an additional eight tin atoms at slightly larger distances (Figure 3a).) Interestingly, the honeycomb net as a bonded entity of Sn atoms also occurs in other transition metal stannides, as for example in CoSn, which was recently investigated by us.[36] The charge density in the (001) plane of $MnSn_2$ (Figure 10a bottom) shows a pronounced local maximum between two Mn atoms (that is a saddle point in a three-dimensional representation of ρ), which is located at the centers of the squares of Sn atoms forming square antiprisms, and we conclude that the Mn−Mn interactions within a chain represent rather strong bonds. Further, we notice that between Mn and

(36) Simak, S. I.; Häussermann, U.; Abrikosov, I. A.; Eriksson, O.; Wills, J. M.; Lidin, S.; Johansson, B. *Phys. Rev. Lett.* **1997**, *79*, 1333.

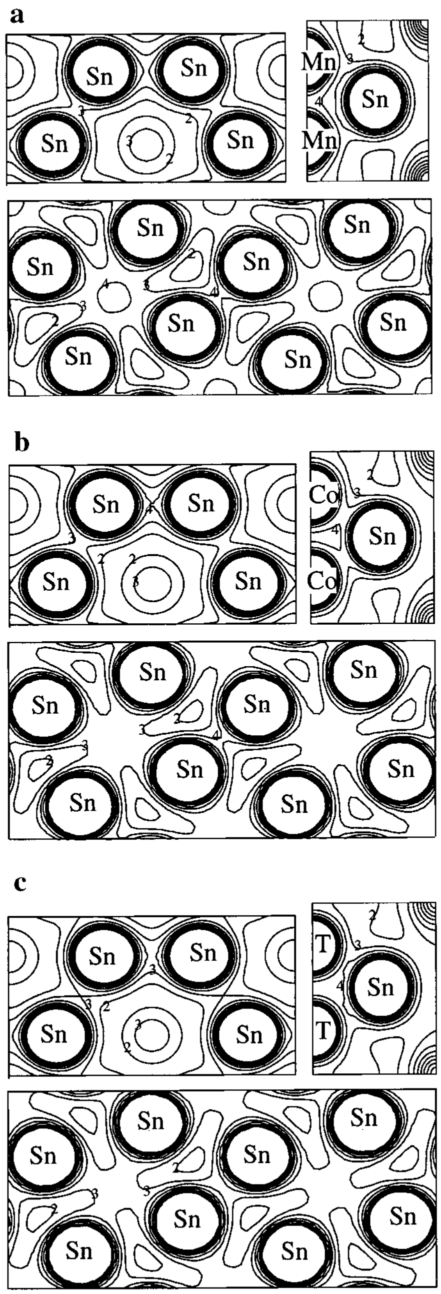

Figure 10. Charge density distributions from FP-LMTO calculations of the plane (220) (top, left), the plane containing a pair of T atoms and a neighboring Sn atom (top, right), and the plane (100) (bottom) in the compounds $MnSn_2$ (a), $CoSn_2$ (b), and $Co_{0.5}Ni_{0.5}Sn_2$ (c) with the $CuAl_2$ structure. The separation of the contours is 0.01 e/bohr^3, the unit of the contours in the plots is 10^{-2} e/b^3 (1 b $\approx$ 0.529 Å).

Sn atoms charge density is almost spherically distributed (Figure 10a top, right). A homogeneous distribution of ρ is usually considered as the result of metallic bonding. Importantly, the $NiMg_2$ and $CuMg_2$ structure types can express exactly the same bonding topology consisting of a homonuclearly bonded E substructure with trigonal planar coordinated E atoms and chains of bonded transition metal atoms (cf. Figure 4b). In $CoSn_2$, VEC is increased by more than 13% compared to $MnSn_2$. The bonding picture for the honeycomb nets of Sn atoms is the same as in $MnSn_2$ (Figure 10b top, left), but the charge density distributions in the other two planes differ strikingly for the two compounds: In the plane (001) the charge density between two Co atoms is considerably lower than between two Mn atoms in $MnSn_2$ (Figure 10b bottom) and the charge density distribution between Co and Sn atoms now shows clear directional bonding (Figure 10b top, right). The remarkable decrease of valence charge density between the T atoms indicates that T−T antibonding electronic states are occupied in $CoSn_2$. Thus the increase of VEC changes the significance of the bonding interactions in such a way that bonding between the T atoms in the one-dimensional chains is weakend and bonding between T and Sn atoms is strengthend, i.e., changes from metallic to directional bonding. In $Co_{0.5}Ni_{0.5}Sn_2$ with the $CuAl_2$ structure, the charge density between pairs of T atoms is even more diminished compared to $CoSn_2$ and additionally the bonding between pairs of Sn atoms (forming the honeycomb net) seems to become weaker (Figure 10c). As a conclusion we consider the loss of bonding or rather the occurrence of antibonding between the T atoms, which is a consequence of the more and more populated d-bands with increasing VEC, as a driving force for the structural transformation of the $CuAl_2$ into the $CoGe_2$ structure. In the latter structure, the chains of T atoms are broken into pairs.

(37) See, e.g.: Pearson, W. B. *The Crystal Chemistry and Physics of Metals and Alloys*; John Wiley & Sons: New York, 1972.

Concluding Remarks

We analyzed in detail the structural sequence $CuMg_2 \rightarrow NiMg_2 \rightarrow CuAl_2 \rightarrow CoGe_2$ which occurs in quasi-binary first-row transition metal distannide systems $T_xT'_{1-x}Sn_2$. The stability of the structures seems to be governed exclusively by electron count or VEC, and we were able to confirm the experimentally determined stability ranges by state-of-the-art computations of total energies. VEC has long been recognized as one of the stability-determining factors for intermetallic systems,[37] but only few systems are known where structural stability of an extended series, like the one we have investigated here, is predominantly governed by this parameter. Unlike semiconducting or insulating compounds, metallic systems can often accommodate a variable electron count over an extended interval until a structural change is observed. For structures with large VEC homogeneity ranges, this is reflected in a more complex picture of the chemical bonding where an interplay of different interactions can balance the changes in electron count. In the investigated systems $T_xT'_{1-x}Sn_2$, this includes, besides "ordinary" T−Sn interactions, a remarkable tendency of the Sn and T atoms to form homonuclear bonds.

Acknowledgment. This work was supported by the Swedish National Science Research Council (NFR) and the Göran Gustafsson Foundation. Further, the Swedish Material Consortium No. 9 is acknowledged. Parts of the calculations were performed at the Swedish National Supercomputer Center (NSC) in Linköping, Sweden.

Supporting Information Available: Tables of anisotropic thermal parameters for all structures and crystallographic data (2 page, print/PDF). Ordering information is given on any current masthead page. See any current masthead page for ordering information and Web access instructions.

JA981347T